Effects of Debye plasmas on two-photon transitions in lithium atoms

S. Paul and Y. K. Ho
Institute of Atomic and Molecular Sciences, Academia Sinica, P.O. Box 23-166, Taipei, Taiwan 106, Republic of China
(Received 19 August 2008; published 27 October 2008)

We have studied two-photon transition rates of atomic lithium within model potential by using the pseudostate summation approach. Transition amplitudes and absorption coefficients have been computed for $2s$-$3s$, $2s$-$4s$, and $2s$-$3d$ transitions with various Debye lengths. In the case of $2s$-$3s$ transition, two-photon transparency vanishes for smaller Debye length. Reverse incident occurred for $2s$-$3d$ transition. Here, we have found a two-photon transparency for lower values of Debye length. These two situations occur due to energy level shifting in the presence of a plasma environment. A detailed description of resonance enhancement frequency and transition amplitude has been analyzed.

DOI: 10.1103/PhysRevA.78.042711 PACS number(s): 34.50.Fa, 32.80.−t, 52.30.−q

I. INTRODUCTION

Plasma screening effect on the plasma embedded atomic systems is an interesting topic which has received wide attention from both theorists and experimentalists [1–17]. The atomic excitation and ionization processes play an essential role in the interpretation of various phenomena associated with astrophysics, hot plasma physics, and experiments performed with positively charged ions. Excitation processes in plasma background are of great interest, because the line emission due to excitation provides detailed information of the physical processes of plasma. A number of studies have been done to investigate the influence of the plasma on scattering processes. A study of inelastic and elastic collision processes [10–12] in strongly coupled plasma has shown that the cross sections are significantly reduced by plasma screening of the electron-ion interaction. Whitten, Lane, and Weisheit [12] have shown that the optically allowed $1s$-$2p$ and $2s$-$2p$ cross sections for electron impact excitation are substantially reduced by the plasma screening, but the $1s$-$2s$ cross section is less sensitive to the plasma effect. The Debye screening effect has played a crucial and significant part in the investigation of plasma environments over the past several decades. Different theoretical methods have been employed along with the Debye screening to study plasma environments [11–22]. Some progress has been made in estimating the influence of the plasma on atomic structure, but information on the scattering process and on various radiative processes is very limited.

Currently, two-photon spectroscopy has became a very powerful technique for studying the excitation level of gases. Since the selection rules are different for two-photon absorption than for one-photon absorption, one can potentially observe electronic states which are not visible in one-photon spectroscopy. There are several attempts to study two-photon transitions between the ground state and the $2s$ state for a free (without any external field) hydrogen atom both experimentally [23,24] and theoretically [25]. Recently, Mon Mohan *et al.* [26] and earlier, Quattropani *et al.* [27] have studied the $1s$-$3s$ transition in an H atom. Transition amplitude and absorption coefficients for a $1s$-$3d$ transition in the H atom are also calculated by Mon Mohan *et al.* [26].

In our earlier work [28], we have observed that the plasma environment has a considerable effect on the frequency of incident photons for resonance enhancement as well as for two-photon transparency. These two frequencies decrease when Debye length is decreased. Presently, we concentrate on the investigation of the plasma screening effect on the two-photon transitions in a lithium atom (within model potential approximation) embedded in weakly coupled plasmas. We have calculated the transition probabilities and absorption coefficients for the $2s$-$3s$, $2s$-$4s$, and $2s$-$3d$ transitions in a plasma embedded lithium atom, which involves evaluation of a summation over intermediate states. The summation of intermediate states is taken care of by using the pseudostate method. Using the pseudostate method we have found excellent converged results, even for a basis size 30, insensitive of basis parameters. The paper is organized as follows. In Sec. II we describe the theory of the present context including model potential, pseudostates technique, and two-photon transition amplitude. In Sec. III we discuss the phenomena of the resonance enhancement and two-photon transparency. The procedure of calculation is presented in Sec. IV. Results are presented in Sec. V with a short discussion and some concluding remarks can be found in Sec. VI. Atomic units are used throughout this paper.

II. THEORY

Our goal is to calculate transition amplitudes and absorption coefficients of a lithium atom in the Debye plasma environment. For our present study, we have considered a model potential of a lithium atom and adopted the pseudostate summation method. Below we show the entire analytical calculation of the current context in three sections.

A. Model potential

In the case of the model potential, the atomic system is regarded as composed of two particles: the valence electron and an atomic core ion whose structure is not considered explicitly. The interaction between the valence electron and core ion is represented by the model potential $V_M(r)$, r being the radial coordinate. A number of analytical model potentials have been discussed in the literature [21]. The basic idea of the model potential $V_M(r)$ is to simulate the multielectron core interaction with the single valence electron by an analytical modification of the Coulomb potential such that

TABLE I. Energy levels for the $1s^2nl$ states of free Li with other theoretical results and experimental data.

nl	Present results	Experimental results [33]	Sahoo *et al.* [29]	Bachau *et al.* [34]	Laughlin *et al.* [35]	Moore *et al.* [36]
$2s$	−0.19814	−0.19814	−0.19814	−0.19814	−0.19815	−0.19809
$3s$	−0.07431	−0.07418	−0.07431	−0.07435	−0.07419	−0.07417
$4s$	−0.03868	−0.03862	−0.03868	−0.03870	−0.03862	−0.03861
$3d$	−0.05557	−0.05561	−0.05557	−0.05558	−0.05562	−0.05561

$$\lim_{r\to\infty}[V_M(r)] = \lim_{r\to\infty}\left(-\frac{\tilde{Z}}{r}\right), \tag{1}$$

$$\lim_{r\to 0}[V_M(r)] = \lim_{r\to 0}\left(-\frac{Z}{r}\right), \tag{2}$$

with Z the atomic number, and $\tilde{Z}$ the ionization stage defined by $\tilde{Z}=Z\text{-}N_c$, where N_c is the number of electrons in the core shell. For the present problem, we considered a model potential of the form

$$V_M(r) = -\frac{1}{r}[(Z-N_c) + N_c(e^{-2\alpha r} + \beta r e^{-2\gamma r})]. \tag{3}$$

α, β, and γ are the model potential parameters. The model potential for the Li atom has been used in an earlier calculation of photoionization cross sections [21]. It is noticed that the energy eigenvalues of a lithium atom with $\alpha=\beta=\gamma=1.6559$ compare well to the experimental data [29]. Under the Debye screening, the valence electron-ion interaction potential for plasma embedded Li can be modeled by [30,31]

$$V(r) = V_M(r)\exp(-r/\lambda_D), \tag{4}$$

where λ_D is the Debye screening length.

B. Pseudostate method

The Hamiltonian of a lithium atom enclosed by a weakly coupled plasma within the model potential in atomic units is

$$H = -\frac{1}{2}\nabla^2 - \frac{1}{r}[(Z-N_c) + N_c(e^{-2\alpha r} + \beta r e^{-2\gamma r})]e^{-r/\lambda_D}, \tag{5}$$

where the values of the model potential parameters α, β, and γ are presented in the above section. We have used a pseudostate method to calculate the energy levels and bound states. The basis function of the pseudostate method are taken of the form (Drachman *et al.* [32])

$$\phi_j = e^{-ar}r^{l+j}Y_{lm}(\theta,\phi), \quad j=0,1,\ldots,N-1, \tag{6}$$

where a is the basis parameter, l is the orbital angular momentum, and N is the basis size. The wave functions are expanded in terms of linear combinations of the basis functions as

$$\Psi_n = \sum_{j=0}^{N-1} C(j,n)\phi_j, \tag{7}$$

and we have

$$\langle n|H|n'\rangle = E_n\Delta_{nn'}, \quad \langle n|n'\rangle = \Delta_{nn'}. \tag{8}$$

The finite-dimensional eigenvalue problem corresponding to the Hamiltonian of a lithium atom (with model potential) in the plasmas field is as follows:

TABLE II. Energy levels of $2s$, $3s$, $4s$, and $3d$ states for Li in the Debye screening plasmas in atomic units. λ_D denotes the Debye length.

λ_D	$E(2s)$	$E(2s)$[a]	$E(3s)$	$E(4s)$	$E(3d)$
25	−0.160220	−0.160220	−0.041237	−0.011021	−0.023001
20	−0.151597	−0.151597	−0.034894	−0.007152	−0.016927
15	−0.137930		−0.025767	−0.002701	−0.008484
10	−0.113089	−0.113089	−0.012276		
6	−0.072380		−0.000346		

[a]Calculated results of Sahoo *et al.* [21].

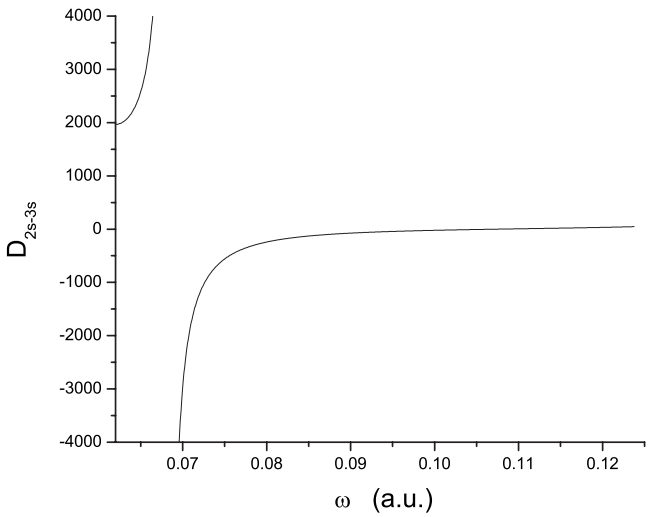

FIG. 1. Two-photon transition amplitude $D_{2s\text{-}3s}$ for the $2s$-$3s$ transition as a function of ω for free Li.

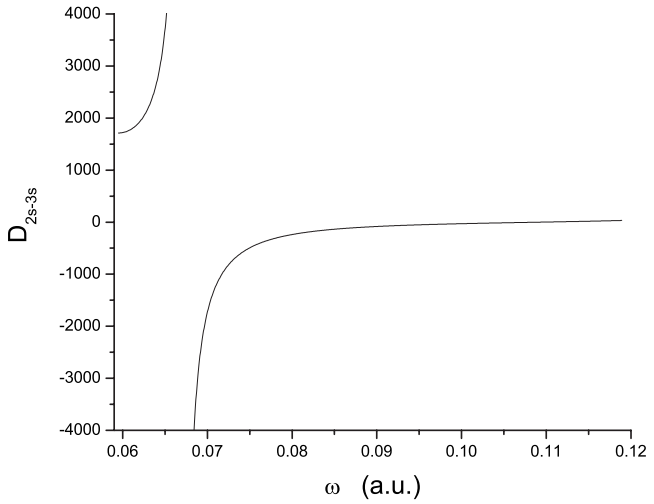

FIG. 2. Same as Fig. 1 but for $\lambda_D=25$.

$$(\underline{H}-E_n\underline{\Delta})|n\rangle=0, \tag{9}$$

where the elements of the Hamiltonian matrix $\underline{H}$ and the overlap matrix $\underline{\Delta}$ are given by the following expression:

$$H_{mn}=\frac{1}{2}\frac{\Gamma(2l+m+n+1)}{(2a)^{2l+m+n+1}}\left[\left(l+\frac{1}{2}\right)(l+1)+\frac{1}{4}(m+n)-\frac{1}{4}(m-n)^2\right]-\Gamma(2l+m+n+2)\times\left[\frac{Z-N_c}{\left(2a+\frac{1}{\lambda_D}\right)^{2l+m+n+2}}+\frac{N_c}{\left(2a+2\alpha+\frac{1}{\lambda_D}\right)^{2l+m+n+2}}+\frac{N_c\beta(2l+m+n+2)}{\left(2a+2\gamma+\frac{1}{\lambda_D}\right)^{2l+m+n+3}}\right], \tag{10}$$

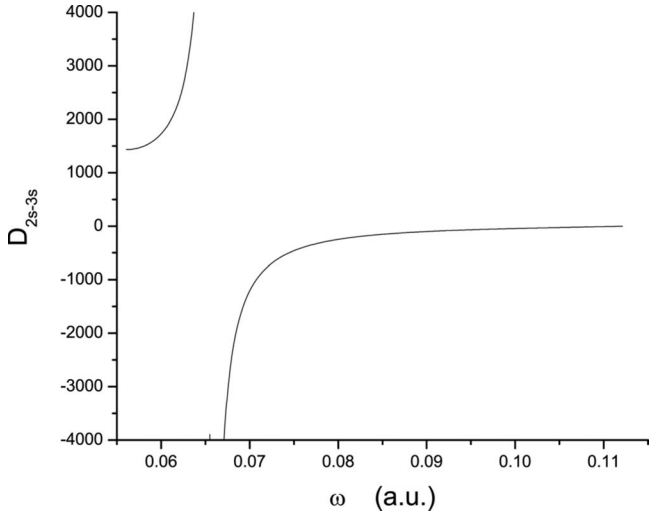

FIG. 3. Same as Fig. 1 but for $\lambda_D=15$.

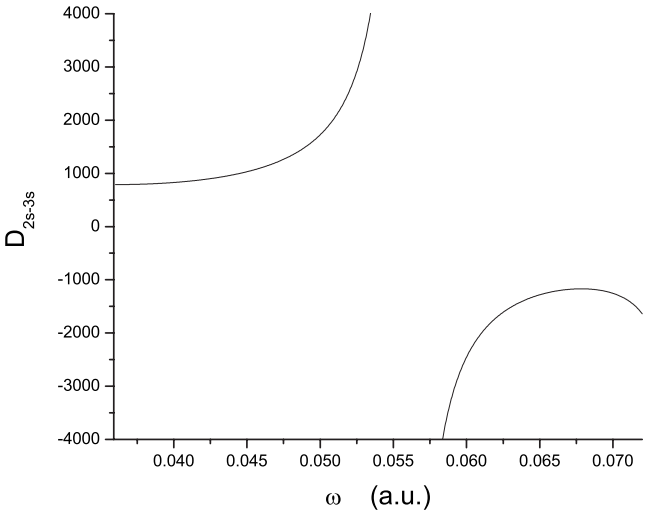

FIG. 4. Same as Fig. 1 but for $\lambda_D=6$.

$$\Delta_{mn}=\frac{\Gamma(2l+m+n+3)}{(2a)^{2l+m+n+3}}. \tag{11}$$

For accurate transition amplitudes, it is essential to calculate converged results with respect to the expansion length N. After obtaining the eigenvalues E_n and eigenfunctions $|n\rangle$ $(=\Psi_n)$, we can continue to compute two-photon transition matrix elements for various transitions.

C. Two-photon transition amplitude

In the length gauge, the two-photon transition probability amplitude $D_{i\text{-}j}$ from an initial state $|i\rangle$ to a final state $|f\rangle$ is given by

$$D_{i\text{-}f}=\frac{3}{2}\sum_n(1+P_{12})\left[\frac{e_{L1}\cdot\langle f|r|n\rangle\langle n|r|i\rangle\cdot e_{L2}}{-E_i+E_n-\nu_2}\right], \tag{12}$$

where e_{L1}, e_{L2} are the polarization of the incident photon and the operator P_{12} interchanges the frequency and polarization

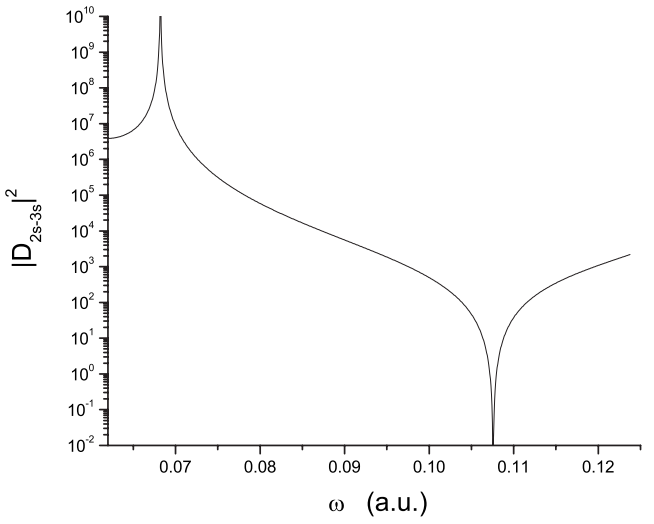

FIG. 5. Dimensionless two-photon absorption coefficient $|D_{2s\text{-}3s}|^2$ for the $2s$-$3s$ transition plotted as a function of ω for free Li.

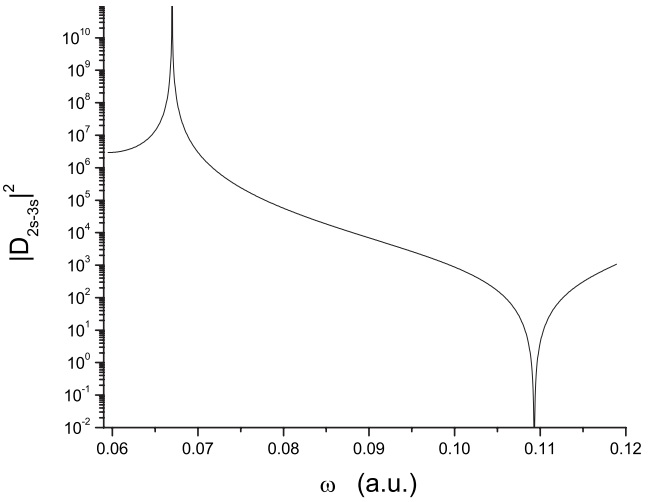

FIG. 6. Same as Fig. 5 but for $\lambda_D=25$.

of two photons. E_i and E_f are the energies of initial and final states. The quantity ν_2 is the energy of the second photon absorbed in the transition; for energy conservation we have the energy of the first photon $\nu_1=E_f-E_i-\nu_2$.

In the case of linearly polarized light the polar axis of the spherical coordinate is taken along the direction of the photon unit polarization vector. In this case we have

$$e_L \cdot r = \sqrt{4\pi/3} r Y_{10}(\theta,\phi), \tag{13}$$

where $Y_{10}(\theta,\phi)$ is the usual spherical harmonic function. The two-photon transition amplitude for the $2s$-js $(j=3,4)$ transition is given by

$$D_{2s\text{-}js} = \frac{1}{2}\sum_n \left[\frac{1}{-E_{2s}+E_n-\omega} + \frac{1}{-E_{js}+E_n+\omega}\right] R^n_{2s} R^n_{js}. \tag{14}$$

Similarly, for the $2s$-$3d$ transition we have

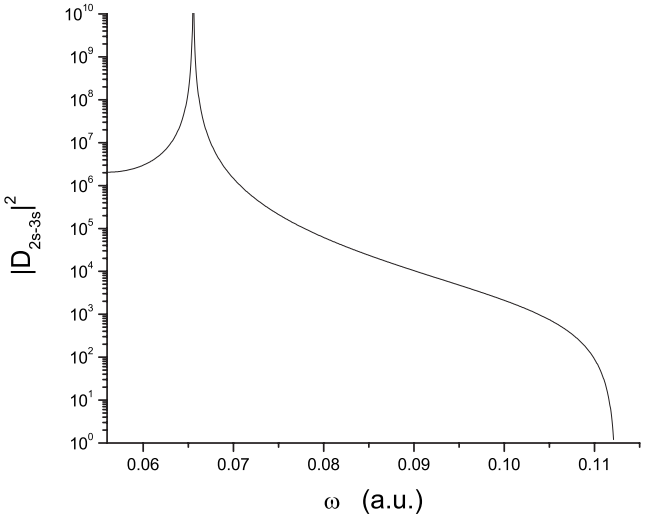

FIG. 7. Same as Fig. 5 but for $\lambda_D=15$.

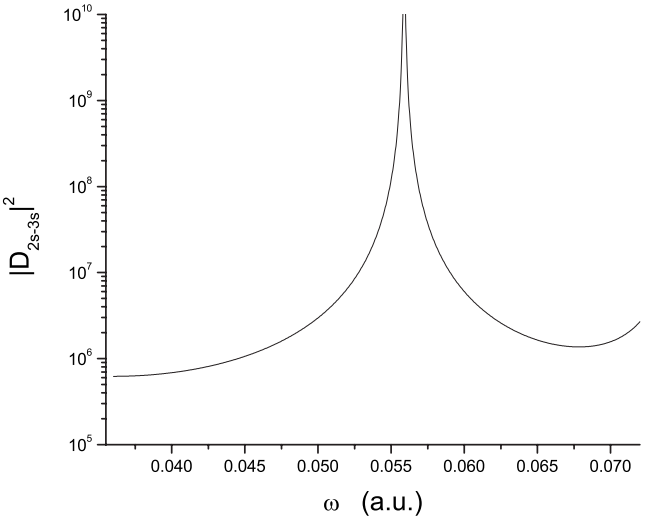

FIG. 8. Same as Fig. 5 but for $\lambda_D=6$.

$$D_{2s\text{-}3d} = \frac{1}{\sqrt{5}}\sum_n \left[\frac{1}{-E_{2s}+E_n-\omega} + \frac{1}{-E_{3d}+E_n+\omega}\right] R^n_{2s} R^n_{3d}, \tag{15}$$

where E_k is the energy eigenvalue of the $|k\rangle$ state and ω is the energy of any one of the two photons. The matrix elements R^n_k are defined as

$$R^n_k = \int_0^\infty r^3 \chi_n \chi_k dr. \tag{16}$$

Here, the functions χ_n are the radial part of the intermediate states Ψ_n (for $l=1$) defined in Eq. (7); χ_k is the radial part of the state $|k\rangle$.

III. RESONANCE ENHANCEMENT AND TRANSPARENCY FREQUENCIES

The two-photon transition matrix elements can be expressed as

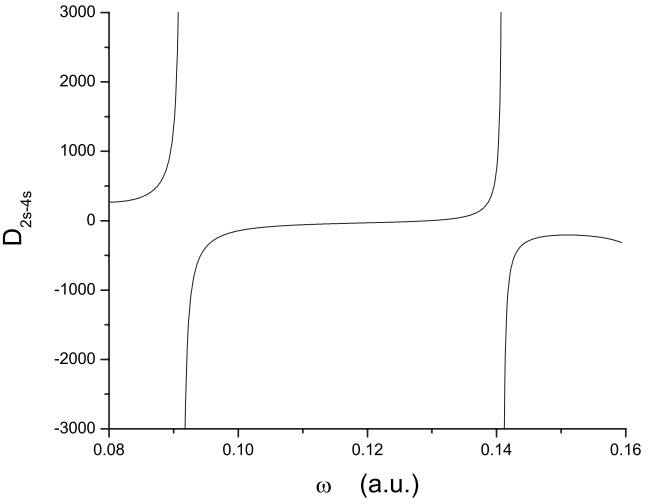

FIG. 9. Two-photon transition amplitude $D_{2s\text{-}4s}$ for the $2s$-$4s$ transition as a function of ω for free Li.

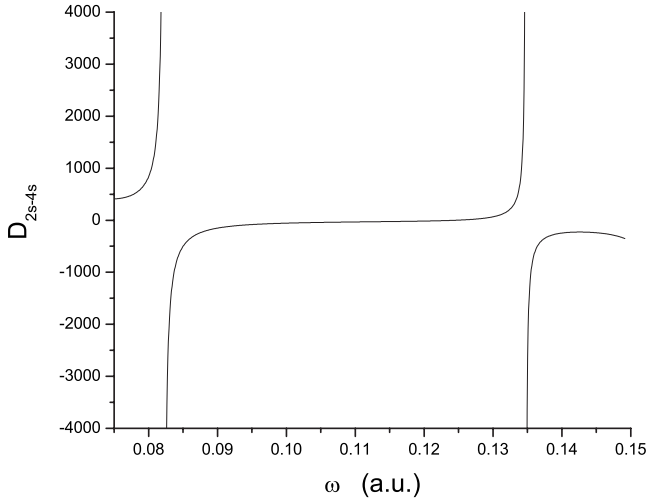

FIG. 10. Same as Fig. 9 but for $\lambda_D=25$.

$$D_{i\text{-}f}=A\sum_n\left[\frac{X_n-Y_n}{(X_n-\omega)(\omega-Y_n)}\right]S_{i\text{-}f}^n, \tag{17}$$

where A is a constant, $X_n=-E_i+E_n$, $Y_n=-E_n+E_f$, and $S_{i\text{-}f}^n=R_i^nR_f^n$. The quantity $(X_n-Y_n)S_{i\text{-}f}^n$ does not depend on ω, it depends only on transition states and Debye length. For a particular transition with fixed Debye length, the two-photon transition amplitude varies with ω due to the factor F_n given by

$$F_n=\frac{1}{(X_n-\omega)(\omega-Y_n)}. \tag{18}$$

The energy gap between transition states $|i\rangle$ and $|f\rangle$ is ΔE_{if}, where

$$\Delta E_{if}=-E_i+E_f. \tag{19}$$

The total energy of the two photons is always fixed and it is equal to ΔE_{if}, so we can consider the energy range of one of the two photons as $I\equiv[\frac{1}{2}\Delta E_{if},\Delta E_{if}]$. The denominator of the factor F_n is equal to zero when $\omega=X_n,Y_n$ for different values of n. Most of the singular points (X_n and Y_n for different n) fall outside the interval I. Only a few of them lie inside the $[\frac{1}{2}\Delta E_{if},\Delta E_{if}]$, and such points are called the resonance enhancement frequencies. Now we examine the sign of the factor F_n. If $X_n<Y_n$, the factor F_n is positive in the interval $[X_n,Y_n]$ and later the interval F_n is negative. The factor F_n is positive in the interval $[Y_n,X_n]$ and negative in the interval aside for $Y_n<X_n$. Again the factor (X_n-Y_n) may be positive or negative, depending on the energy levels. Sometimes we get that all transition amplitudes with respect to ω have the same sign. Occasionally transition amplitudes increase slowly from negative to positive. In the latter case, there exists a frequency for which the amplitude vanishes; we expect a two-photon transparency to be observed at such a frequency.

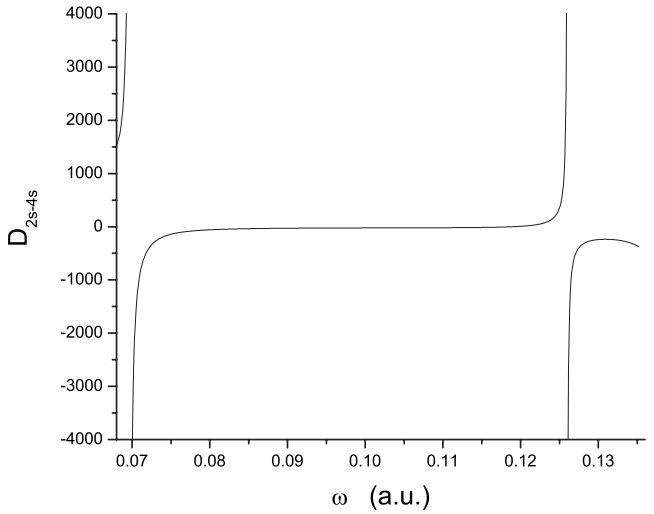

FIG. 11. Same as Fig. 9 but for $\lambda_D=15$.

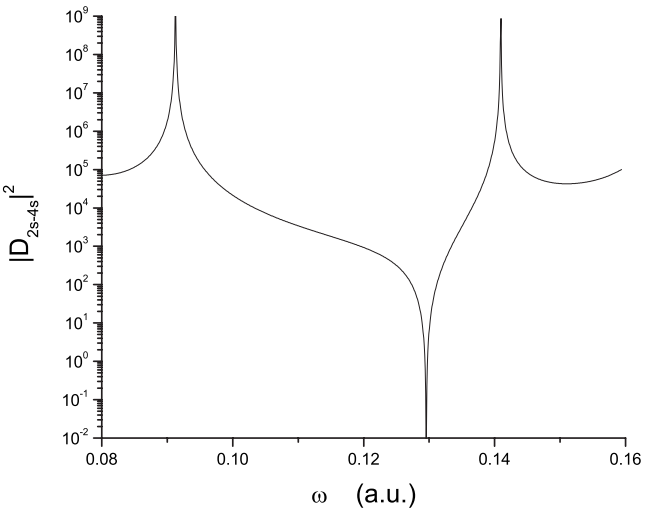

FIG. 12. Dimensionless two-photon absorption coefficient $|D_{2s\text{-}4s}|^2$ for the $2s$-$4s$ transition plotted as a function of ω for free Li.

IV. CALCULATION

To compute transition amplitudes and absorption coefficients of $2s$-$3s$, $2s$-$4s$, and $2s$-$3d$ transitions in a lithium

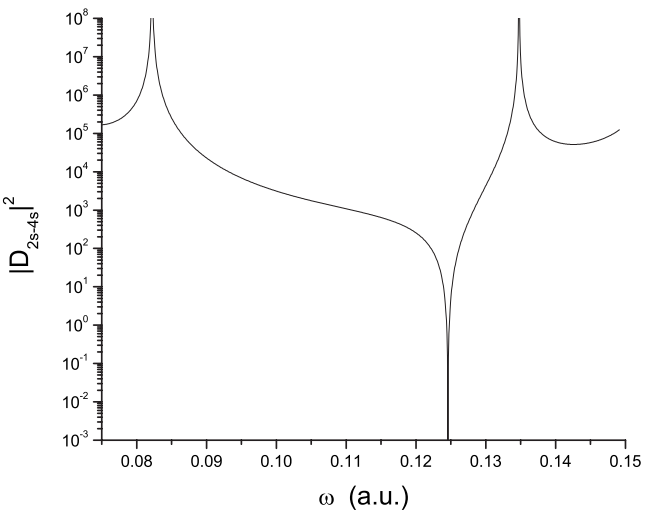

FIG. 13. Same as Fig. 12 but for $\lambda_D=25$.

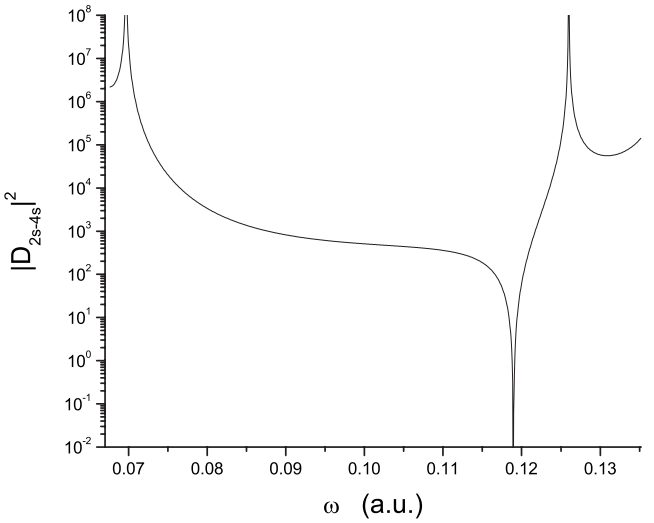

FIG. 14. Same as Fig. 12 but for $\lambda_D=15$.

atom embedded in weakly coupled plasma, we have calculated the $2s$, $3s$, $4s$, and $3d$ bound states, intermediate p states, and corresponding energy eigenvalues by using the pseudostate summation technique. There are two parameters in the pseudostate method; they are "a" (the basis parameter) and N (the number of state in the basis). In our earlier work [28], we had reported that results are not too sensitive to the values of the basis parameter a when the basis size N is sufficiently large. Presently, we have obtained converged results for $a=1$ and $N=30$. We have worked out transition amplitudes and absorption coefficients for various Debye lengths ($\lambda_D=\infty$, 25, 20, 15, etc.). All the singular points have been evaluated in the $2s$-$3d$ transition for $\lambda_D=16$ and 17.

V. RESULTS AND DISCUSSION

The energies of free Li are shown in Table I and are compared with experimental data [33] and other theoretical

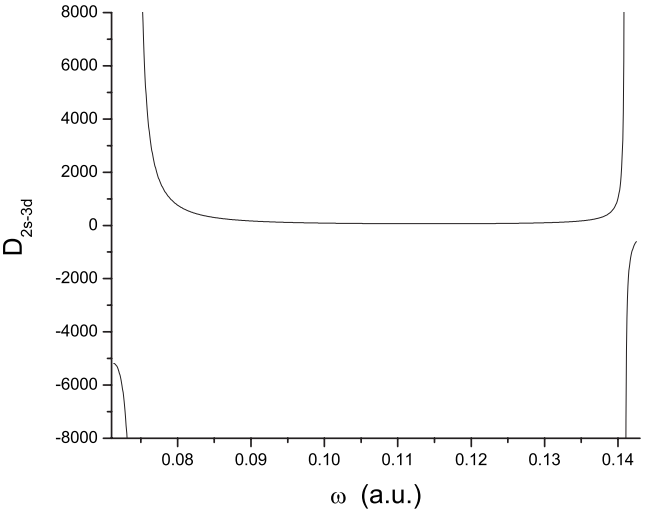

FIG. 15. Two-photon transition amplitude $D_{2s\text{-}3d}$ for the $2s$-$3d$ transition as a function of ω for free Li.

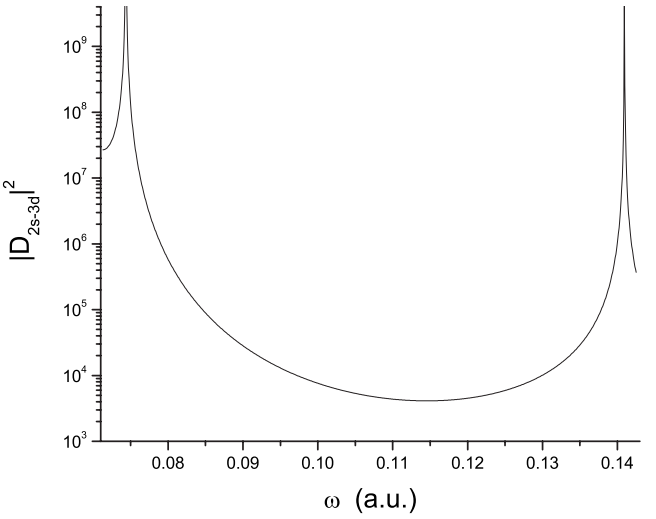

FIG. 16. Dimensionless two-photon absorption coefficient $|D_{2s\text{-}3d}|^2$ for the $2s$-$3d$ transition plotted as a function of ω for free Li.

results [29,34–36]. Our calculated energy eigenvalues for $2s$, $3s$, $4s$, and $3d$ states for various Debye lengths are presented in Table II with the available theoretical results. Our calculated energy eigenvalues are the same as those calculated results of Sahoo *et al.* [29]. They used an orthonormal Laguerre-type basis to study energy levels of a lithium atom. In this section, we have presented transition amplitudes and absorption coefficients of $2s$-$3s$, $2s$-$4s$, and $2s$-$3d$ transitions in a lithium atom embedded in weak plasma. Figures 1–4 represent the transition amplitudes $D_{2s\text{-}3s}$ for a lithium atom in the presence of a plasma field for Debye length ∞, 25, 15, and 6. From the figures, we observe that two-photon transparency disappears with the reduced value of λ_D. We observe a transparency for the free field case and for $\lambda_D=25$, but the transparency vanishes for $\lambda_D=6$, although resonance enhancements remain present. The dimensionless absorption coefficients $|D_{2s\text{-}3s}|^2$ for the process described above are shown in Figs. 5–8.

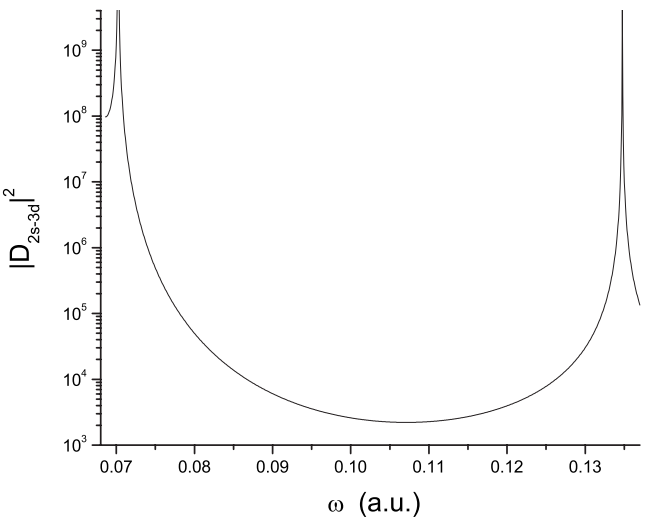

FIG. 17. Same as Fig. 15 but for $\lambda_D=25$.

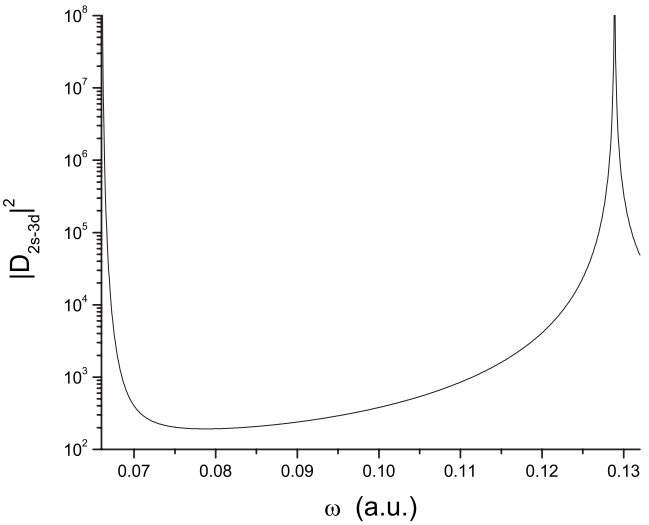

FIG. 18. Same as Fig. 15 but for $\lambda_D=17$.

For the $2s$-$4s$ transition in Li, the transition amplitudes are reported in Figs. 9–11 for different λ_D. Here we find two resonance enhancement frequencies and one two-photon transparency frequency with various Debye lengths. The absorption coefficients for the $2s$-$4s$ transition are presented in Figs 12–14. The most interesting feature is the $2s$-$3d$ transition in Li with different Debye lengths.

Figure 15 shows that in case of the $2s$-$3d$ transition in free Li, there are two resonance enhancement frequencies but transparency is absent. The curve of the absorption coefficient (Fig. 16) shows that in between two resonance enhancement points the shape of the curve is likely U and the deep has became deeper with the decrease of λ_D as shown in Figs. 17 and 18. The process continued up to $\lambda_D=16.98$ (approximately). For $\lambda_D=16.97$ (approximately), a two-photon transparency starts to appear. Figures 19 and 20 show transition amplitudes for $\lambda_D=25$ and 17. Figures 21 and 22 represent transition amplitudes and absorption coefficients, respectively, where two-photon transparency has been found for $\lambda_D=16$.

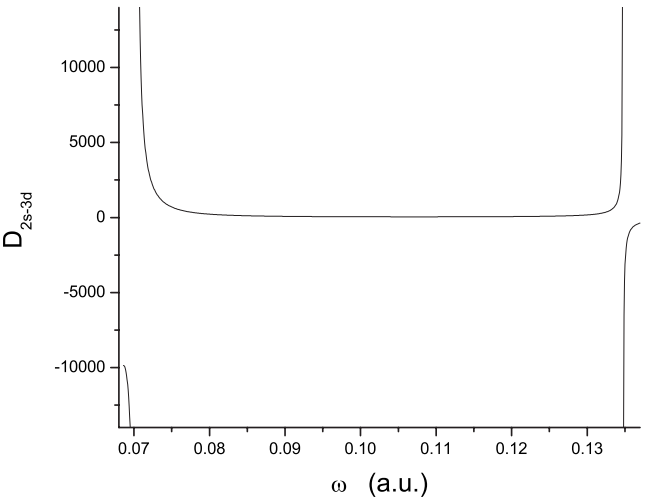

FIG. 19. Same as Figure 16 but for $\lambda_D=25$.

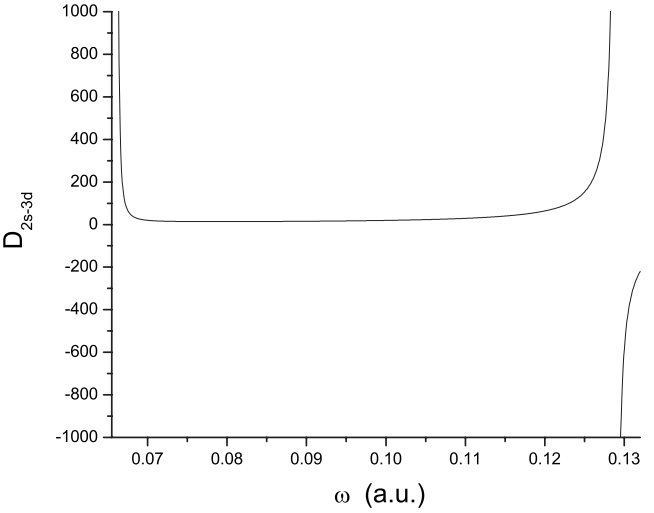

FIG. 20. Same as Fig. 16 but for $\lambda_D=17$.

In Tables III and IV, we have produced all the singular points X_n, Y_n (as defined in Sec. III) for the $2s$-$3d$ transition in a Li atom along with $S^n_{i\text{-}f}$ for $\lambda_D=16$ and 17, respectively. Equation (17) can be written as

$$D_{i\text{-}f}=\sum_n \frac{B_n}{F_n}=\sum_n \zeta_n, \tag{20}$$

where $B_n=A(X_n-Y_n)S^n_{i\text{-}f}$. If α and β are two resonance enhancement points, i.e., α and β belong to the union of the two sets $\{X_n\}$ and $\{Y_n\}$, for certain values of n, say n_1 and n_2. The matrix elements ζ_{n_1} and ζ_{n_2} dominate the elements ζ_n for all other values of n when ω is closed to α and β, respectively. The sign of ζ_{n_1} and ζ_{n_2} in the region close to α and β, respectively, depends only on B_n, or particularly, on X_n-Y_n because F_{n_1} and F_{n_2} have a specific sign as discussed in Sec. III.

In Figs. 23 and 24, we have presented the singular points, the range of ω, i.e., $[\Delta E/2,\Delta E]$ and the sign of F_1 and F_2 for the $2s$-$3d$ transition in a Li atom with Debye length 16 and

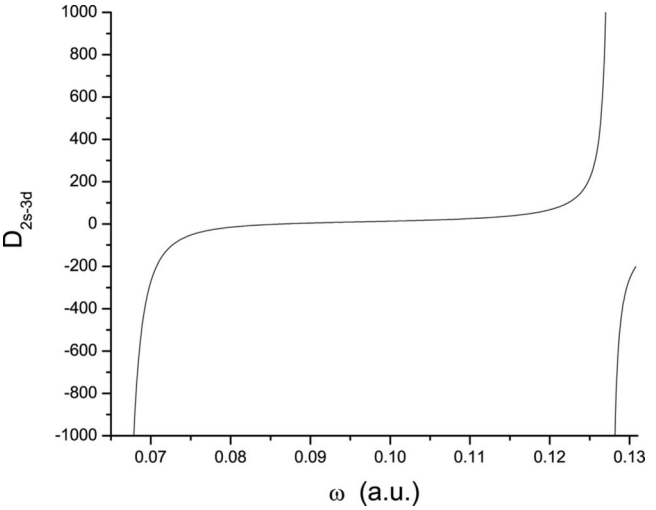

FIG. 21. Same as Fig. 15 but for $\lambda_D=16$.

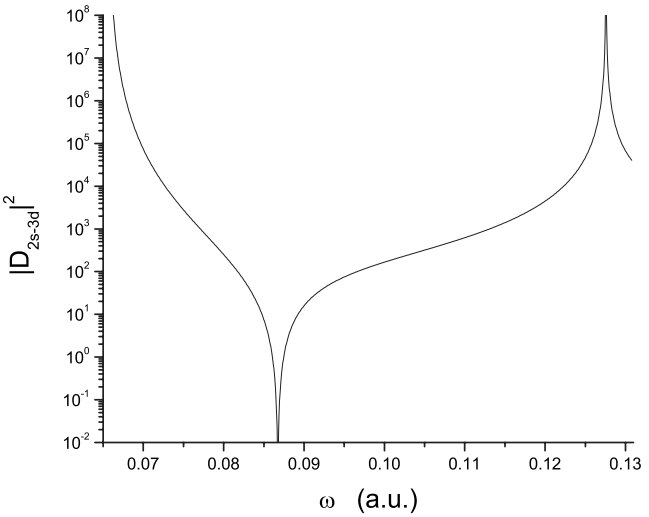

FIG. 22. Same as Fig. 16 but for $\lambda_D=16$.

TABLE III. The singular points X_n, Y_n and matrix elements $S^n_{2s\text{-}3d}$ for the $2s$-$3d$ transition in a Li atom with the Debye length 16. The bold face numbers are resonance enhancement frequencies.

n	X_n (a.u.)	Y_n (a.u.)	X_n-Y_n (a.u.)	$S^n_{2s\text{-}3d}$ (a.u.)
1	**0.065805**	0.065061	0.000744	17.575051
2	**0.127566**	0.003301	0.124264	1.313677
3	0.141042	−0.010175	0.151216	−0.239092
4	0.146884	−0.016017	0.162902	−0.173070
5	0.156146	−0.025279	0.181425	−0.137175
6	0.168888	−0.038021	0.206910	−0.095015
7	0.185220	−0.054353	0.239573	−0.066711
8	0.205435	−0.074568	0.280003	−0.042787
9	0.229977	−0.099110	0.329087	−0.029923
10	0.259451	−0.128584	0.388035	−0.018018
11	0.294650	−0.163784	0.458434	−0.013100
12	0.336607	−0.205740	0.542347	−0.007202
13	0.386659	−0.255792	0.642451	−0.005737
14	0.446559	−0.315693	0.762252	−0.002686
15	0.518619	−0.387752	0.906371	−0.002554
16	0.605934	−0.475067	1.081000	−0.000871
17	0.712707	−0.581841	1.294548	−0.001169
18	0.844771	−0.713905	1.558676	−0.000184
19	1.010378	−0.879511	1.889890	−0.000556
20	1.221534	−1.090667	2.312201	−0.000044
21	1.496213	−1.365346	2.861559	−0.000275
22	1.862350	−1.731483	3.593832	−0.000092
23	2.365202	−2.234336	4.599538	−0.000140
24	3.082180	−2.951313	6.033492	0.000076
25	4.154532	−4.023665	8.178197	−0.000069
26	5.863333	−5.732466	11.595799	0.000044
27	8.835890	−8.705022	17.540911	−0.000029
28	14.715057	−14.584190	29.2999248	0.000016
29	29.168625	−29.037759	58.206385	−0.000007
30	86.720695	−86.589829	173.310524	0.000002

TABLE IV. The singular points X_n, Y_n and matrix elements $S^n_{2s\text{-}3d}$ for the $2s$-$3d$ transition in a Li atom with the Debye length 17. The bold face numbers are resonance enhancement frequencies.

n	X_n (a.u.)	Y_n (a.u.)	X_n-Y_n (a.u.)	$S^n_{2s\text{-}3d}$ (a.u.)
1	0.066021	**0.066036**	−0.000015	17.673155
2	**0.128892**	0.003165	0.125727	1.420721
3	0.143391	−0.011334	0.154725	−0.243423
4	0.149297	−0.017240	0.166538	−0.162449
5	0.158458	−0.026401	0.184859	−0.133400
6	0.171125	−0.039068	0.210194	−0.094701
7	0.187392	−0.055335	0.242727	−0.066476
8	0.207544	−0.075488	0.283033	−0.043582
9	0.232024	−0.099967	0.331991	−0.030004
10	0.261432	−0.129376	0.390809	−0.018714
11	0.296562	−0.164505	0.461067	−0.164505
12	0.338442	−0.206385	0.542347	−0.007679
13	0.388410	−0.256353	0.644763	−0.005659
14	0.448217	−0.316160	0.764377	−0.002995
15	0.520173	−0.388117	0.908290	−0.002450
16	0.607373	−0.475317	1.082689	−0.001072
17	0.714020	−0.581964	1.295984	−0.001071
18	0.845944	−0.713888	1.559833	−0.000314
19	1.011398	−0.879341	1.890739	−0.000476
20	1.222387	−1.090330	2.312717	−0.000040
21	1.496884	−1.364828	2.861712	−0.000216
22	1.862825	−1.730769	3.593594	0.000038
23	2.365466	−2.233410	4.598876	−0.000100
24	3.082212	−2.950156	4.419519	0.000044
25	4.154306	−4.022249	8.176555	−0.000046
26	5.862796	−5.730740	11.593536	0.000028
27	8.834927	−8.702871	17.537798	−0.000019
28	14.713357	−14.58130	29.294658	0.000010
29	29.165575	−29.03351	58.199094	−0.000005
30	86.715865	−86.58381	173.299674	0.000001

17, respectively. X_1, X_2 are resonance enhancement frequencies for $\lambda_D=16$, and Y_1, X_2 are those for the Debye length 17. Tables III and IV presented the data of X_n, Y_n, X_n-Y_n, and $S^n_{2s\text{-}3d}$ for Debye length 16 and 17, respectively. The bold face numbers in the Tables III and IV indicate resonance enhancement frequencies. Figure 23 and Table III show that the values of $D_{2s\text{-}3d}$ are negative when the values of ω are greater than and close to X_1, and $D_{2s\text{-}3d}$ is positive when ω is less than and close to X_2 for $\lambda_D=16$, because $X_n-Y_n>0$ for all n. In this case transition amplitudes are increased from negative to positive. Similarly, Fig. 24 and Table IV show that the values of $D_{2s\text{-}3d}$ are positive when the values of ω are greater than and close to Y_1 because $X_1-Y_1<0$, and $D_{2s\text{-}3d}$ is positive when ω is less than and close to X_2 because $X_n-Y_n>0$ for $n>1$. In this case, the transition amplitude is positive in both regions, close to the two resonance enhancement points. The two figures indicate that the two-photon transparency occur for $\lambda_D=16$, due to X_1-Y_1 [i.e., $-E(2s)$

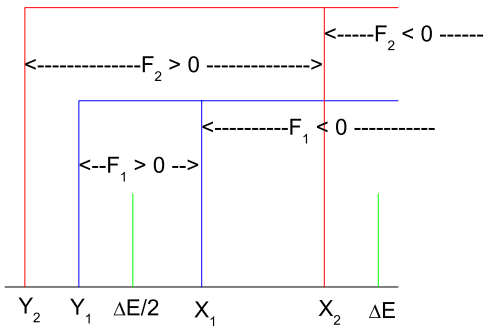

FIG. 23. (Color online) Resonance enhancement frequencies, range of ω, and sign of F_1, F_2 for $\lambda_D=16$.

$-E(3d)+E(2p)$, the energy levels of $2s$, $3d$, and $2p$ states] being positive. Hence, the sign of the transition amplitude (for which transparency occurs) depends only on the sign of X_1-Y_1. The value, as well as the sign of X_1-Y_1, is changed with the shift of energy eigenvalues of $2s$, $3d$, and $2p$ states for different Debye lengths. The values of ω_t and ω_{r1}, ω_{r2} (the first and second resonance enhancement frequencies) for the $2s$-$4s$ transition with various Debye lengths are given in Table V. A variation of ω_t, ω_{r1}, and ω_{r2} for the $2s$-$4s$ transition with respect to the reciprocal of Debye length is presented in Fig. 25. We have presented the values of ω_t for the $2s$-$3d$ transition with $\lambda_D \leqslant 16.968\,75$ as a tabulated form in Table VI and graphically in Fig. 26. Figures 25 and 26 show that the values of ω_t decrease for the $2s$-$4s$ transition and increase for the $2s$-$3d$ transition when λ_D is decreased.

VI. CONCLUSION

We have employed the pseudostate summation technique and model potential to study two-photon transition amplitudes and absorption coefficients for $2s$-$3s$, $2s$-$4s$, and $2s$-$3d$ transitions in a Li atom embedded in plasmas. Calculated results imply that the Debye length as well as plasma environment have considerable effect on the phenomena of resonance enhancement and two-photon transparency. In the case of the $2s$-$3s$ transition, two-photon transparency disappears for lesser values of λ_D. A reverse incident occurs for the $2s$-$3d$ transition. Here, a two-photon transparency appears for smaller values of λ_D (approximately, $\lambda_D \leqslant 16.97$), while there are no two-photon transparencies for free field and

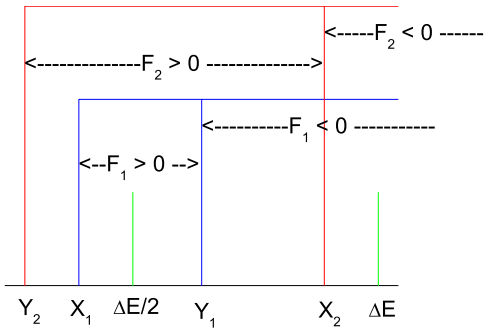

FIG. 24. (Color online) Resonance enhancement frequencies, range of ω, and sign of F_1, F_2 for $\lambda_D=17$.

TABLE V. The values of the two-photon transparency ω_t, first resonance enhancement frequency ω_{r1}, and second resonance enhancement frequency ω_{r2} for the $2s$-$4s$ transition in the lithium atom in the plasma field. λ_D denotes the Debye length.

λ_D	ω_t (a.u.)	ω_{r1} (a.u.)	ω_{r2} (a.u.)
∞	0.1296	0.0913	0.1410
25	0.1246	0.0822	0.1347
20	0.1225	0.0779	0.1318
15	0.1189	0.0696	0.1260

larger values of λ_D (approximately, $\lambda_D \geqslant 16.98$). In the presence of plasma fields, energy levels of atomic lithium are shifted by which these types of interesting features happened. We wish to underline the treatment of the plasma's influence on the two-photon transition in a lithium atom. Here, the net electrostatic interaction due to the specific configuration of the background particles existing at the time of excitation is replaced by the average net interaction of an appropriate distribution of configurations. The approximation is expected to be accurate when the transition duration is much larger than the characteristic plasma response time. Without this simplification, the static plasma screening formula is not reliable. Thus, the dynamic motion of the plasma electrons has to be considered in order to investigate the plasma screening effects on the two-photon transitions. The effects can be considered qualitatively by the introduction of a plasma dielectric function [37]. The effects may be important for high-density plasma or for transitions with low excitation energy, but for low-density plasma or transition with high excitation energy, the effect can be neglected. Thus the static plasma screening formula obtained by the Debye-Hückel model overestimates the plasma screening effects on the transition process in dense plasma for low excitation en-

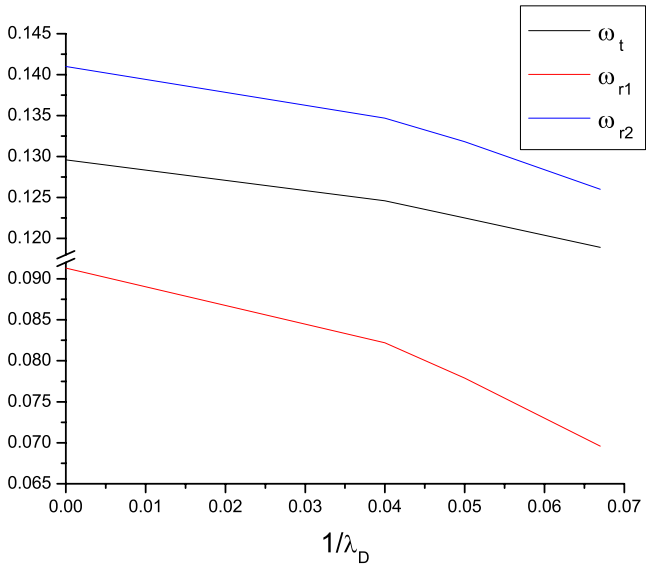

FIG. 25. (Color online) Shift of the two-photon transparency frequency ω_t and the resonance enhancement frequencies ω_{r1}, ω_{r2} for the $2s$-$4s$ transition as a function of the reciprocal of the Debye length.

TABLE VI. The values of the two-photon transparency frequency ω_t for the $2s$-$3d$ transition in the lithium atom in the plasma field. λ_D denotes the Debye length.

λ_D	ω_t (a.u.)
16.984375	Absent
16.96875	0.0681
16.9375	0.0702
16.875	0.0727
16.75	0.0760
16.5	0.0802
16	0.0867
15	0.0957

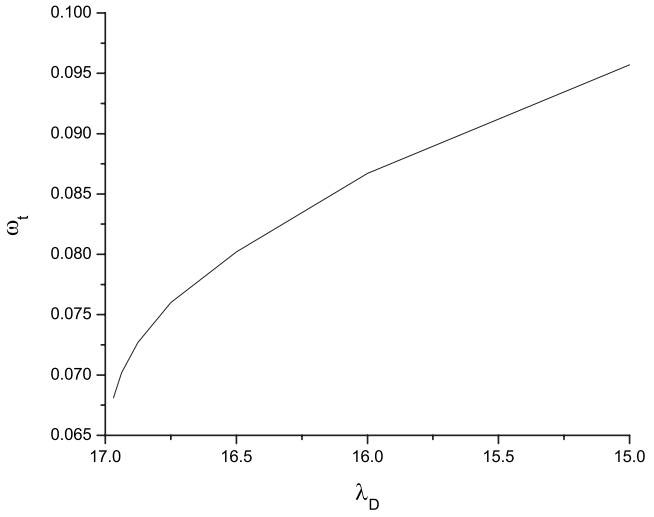

FIG. 26. Shift of the two-photon transparency frequency ω_t for the $2s$-$3d$ transition as a function of the Debye length.

ergy. It is, indeed, necessary to recalculate the two-photon transition amplitude in dense plasma on the basis of kinetic plasma theory, which, in particular, permits one to account the collective plasma effects, namely, dynamic screening along with plasma fluctuations. Even though the differences in the amplitudes include the dynamic and static screening effect is expected not to be too large, the correct information of two-photon transition amplitude is essential to deduce an accurate description of the two-photon transition amplitudes and electron distributions in all energy ranges. The static screening result presented here is subject to the condition that the plasma is a thermodynamically equilibrium plasma and neglects the contributions from ions in plasma since electrons provide more effective shielding than ions. With the change of plasma conditions, a significant variation in two-photon transition amplitudes may take place. In the static plasma screening, we observe that the two-photon transition amplitude is mainly determined by the Debye length, which in turn is determined by the plasma temperature and density. With an increase in plasma density at a given temperature, the Debye length decreases and, thus the effects from plasma temperature and density cannot be neglected. Finally, we mention that interested readers in dynamic screening effects are referred to the references where such effects were studied for electron capture processes [38,39], and for constructing the dynamic screening potential using the plasmas dielectric functions in a calculation of electron capture cross sections [40]. Line broadening is another interesting feature of transition phenomenon. Because of the complexity of line broadening calculations, the analysis of line broadening is beyond the scope of our present context. In this paper, we have considered a lithium atom, but the present approach can also be extended to study resonance enhancement and two-photon transparency of other atoms in plasma environments by using model potentials.

ACKNOWLEDGMENT

The authors would like to thankfully acknowledge financial support by the National Science Council of Taiwan, Republic of China.

[1] G. J. Hatton, N. F. Lane, and J. C. Weisheit, J. Phys. B **14**, 4879 (1981).
[2] N. C. Deb and N. C. Sil, J. Phys. B **17**, 3587 (1984).
[3] J. C. Weisheit, Adv. At. Mol. Phys. **25**, 101 (1988).
[4] R. K. Janev, L. P. Presnyakov, and V. P. Shevelko, *Physics of Highly Charged Ions* (Springer-Verlag, Berlin, 1985), Chap. 3.
[5] D. Salzmann, J. Stein, I. B. Goldberg, and R. H. Pratt, Phys. Rev. A **44**, 1270 (1991).
[6] V. P. Shevelko and L. A. Vainshtein, *Atomic Physics for Hot Plasmas* (Institute of Physics, London, 1993), Chap. 1.
[7] F. A. Gutierrez and J. Diaz-Valdes, J. Phys. B **27**, 593 (1994).
[8] R. Brandenburg, J. Schweinzer, S. Fiedler, F. Aumayr, and H. P. Winter, Plasma Phys. Controlled Fusion **41**, 471 (1999).
[9] L. B. Zhao and Y. K. Ho, Phys. Plasmas **11**, 1695 (2004).
[10] W. Hong and Y. D. Jung, Phys. Plasmas **3**, 2457 (1996).
[11] Y. D. Jung, Phys. Fluids B **5**, 3432 (1993); Phys. Plasmas **2**, 332 (1995); **2**, 987 (1995); **5**, 3781 (1998); **5**, 4456 (1998).
[12] J. S. Yoon and Y. D. Jung, Phys. Plasmas **3**, 3291 (1996).
[13] U. Gupta and A. K. Rajagopal, Phys. Rep. **87**, 259 (1982).
[14] B. L. Whitten, N. F. Lane, and J. C. Weisheit, Phys. Rev. A **29**, 945 (1984).
[15] M. R. Flannery and E. Oks, Eur. Phys. J. D **47**, 27 (2008).
[16] L. Liu, J. G. Wang, and R. K. Janev, Phys. Rev. A **77**, 032709 (2008); **77**, 042712 (2008).
[17] M. S. Pindzola, S. D. Loch, J. Colgan, and C. J. Fontes, Phys. Rev. A **77**, 062707 (2008).
[18] C. Stubbins, Phys. Rev. A **48**, 220 (1993).
[19] P. M. Bellan, Phys. Plasmas **11**, 3368 (2004).
[20] A. C. H. Yu and Y. K. Ho, Phys. Plasmas **12**, 043302 (2005).
[21] S. Sahoo and Y. K. Ho, Phys. Plasmas **13**, 063301 (2006).
[22] S. Kar and Y. K. Ho, Phys. Plasmas **15**, 013301 (2008).
[23] T. W. Hansch, S. A. Lee, R. Wallenstein, and C. Wieman, Phys.

Rev. Lett. **34**, 307 (1975).
[24] S. A. Lee, R. Wallenstein, and T. W. Hansch, Phys. Rev. Lett. **35**, 1262 (1975).
[25] F. Bassani, J. J. Forney, and A. Quattropani, Phys. Rev. Lett. **39**, 1070 (1977).
[26] R. Kundliya, V. Prasad, and Man Mohan, J. Phys. B **33**, 5263 (2000).
[27] A. Quattropani, F. Bassani, and S. Carillo, Phys. Rev. A **25**, 3079 (1982).
[28] S. Paul and Y. K. Ho, Phys. Plasmas **15**, 073301 (2008).
[29] S. Sahoo and Y. K. Ho, J. Phys. B **33**, 2195 (2000); Phys. Rev. A **65**, 015403 (2001); Chin. J. Physiol. **43**, 58 (2005).
[30] J. M. Gil, P. Martel, E. Minguez, J. G. Rubiano, R. Rodriguez, and F. H. Ruano, J. Quant. Spectrosc. Radiat. Transf. **75**, 539 (2002).
[31] C. A. Rouse, Phys. Rev. A **4**, 90 (1971).
[32] R. J. Drachman, A. K. Bhatia, and A. A. Shabazz, Phys. Rev. A **42**, 6333 (1990).
[33] S. Bashkin and J. O. Stoner, *Atomic Energy Levels and Grotrian Diagrams* (North-Holland, Amsterdam, 1975), Vol. 1.
[34] H. Bachau, P. Galan, and F. Martin, Phys. Rev. A **41**, 3534 (1990).
[35] C. Laughlin and G. A. Victor, *Atomic Physics* (Plenum, New York, 1972), Vol. 3, p. 247.
[36] R. A. Moore, J. D. Reid, W. T. Hyde, and C. F. Liu, J. Phys. B **14**, 9 (1981).
[37] Y. D. Jung, Phys. Rev. E **55**, 3369 (1997); C. G. Kim and Y. D. Jung, Phys. Plasmas **5**, 3493 (1998).
[38] C. G. Kim and Y. D. Jung, Phys. Plasmas **5**, 2806 (1998).
[39] Y. D. Jung and J. S. Yoon, Phys. Plasmas **6**, 3674 (1999).
[40] C. G. Kim and Y. D. Jung, Plasma Phys. Controlled Fusion **46**, 1493 (2004).